

# Theoretical and experimental studies of the dissociation dynamics of methaniminium cation, $\text{CH}_2\text{NH}_2^+ \rightarrow \text{CHNH}^+ + \text{H}_2$ : Reaction path bifurcation

Tae Hoon Choi, Sang Tae Park, and Myung Soo Kim<sup>a)</sup>

National Creative Research Initiative for Control of Reaction Dynamics and School of Chemistry,  
Seoul National University, Seoul 151-742, Korea

(Received 20 July 2000; accepted 22 January 2001)

The unimolecular dissociation of  $\text{CH}_2\text{NH}_2^+$  has been investigated experimentally and theoretically. Kinetic energy release distribution was obtained by analyzing the mass-analyzed ion kinetic energy profile. Critical configurations along the reaction path were investigated by electronic structure calculations at the HF, MP2, QCISD, and B3LYP levels using the 6-31G\*\* and 6-311+G\*\* basis sets. Reaction path bifurcation was observed at all the levels. The bifurcation point was in the entrance region (before the transition state) at the HF level. This point moved to the exit region when the electron correlation effect was included at the MP2, QCISD, and B3LYP levels. A global potential energy surface incorporating this bifurcation feature was constructed by interpolation at the MP2/6-311+G\*\* level. Classical trajectories were calculated on this surface and product mode-specific energies were evaluated. Based on these data, various experimental observations, lack of hydrogen scrambling in particular, could be adequately explained. © 2001 American Institute of Physics. [DOI: 10.1063/1.1355309]

## I. INTRODUCTION

Theoretical study of the product energy partitioning, the kinetic energy release (KER) in particular, has contributed tremendously to the elucidation of the dissociation dynamics of polyatomic ions.<sup>1–9</sup> It is now well established that the statistical–dynamical theories such as the phase space theory<sup>2–4,10,11</sup> provide a decent description of the kinetic energy release in the ionic dissociation occurring without a significant reverse barrier. Recently, classical trajectory calculations have become popular to understand the energy partitioning in reactions with large reverse barriers such as rearrangements for which the statistical theories are inherently inappropriate.<sup>7–9</sup> Calculation of a classical trajectory<sup>12,13</sup> requires information on the potential energy along the reaction path and in its vicinity. The approach taken in this laboratory has been to carry out classical trajectory calculations on a potential energy surface (PES) constructed by interpolation of local harmonic potentials obtained by electronic structure calculations at many (300–500) configuration points near the reaction path.<sup>14,15</sup> It is well established now that the interpolation scheme provides a PES which is a faithful representation of the authentic quantum-chemical surface.<sup>15–17</sup> In the case of the  $\text{H}_2$  loss from  $\text{CH}_2\text{OH}^+$ , which is a prototype dehydrogenation reaction of a polyatomic ion, the experimental kinetic energy release and its change upon deuterium substitution could be accounted for almost quantitatively by the classical trajectory method on the interpolated PESs.<sup>14,18</sup>

Loss of  $\text{H}_2$  from the methaniminium ion,  $\text{CH}_2\text{NH}_2^+$ , is another prototype dehydrogenation reaction which has been widely investigated experimentally and theoretically<sup>19–25</sup>



The experimental observation that  $\text{CH}_2\text{ND}_2^+$  eliminated HD only has established that hydrogen scrambling does not occur and that the reaction proceeds via synchronous 1, 2-elimination.<sup>19,23,25</sup> The early *ab initio* study at the Hartree–Fock (HF) level with the 6-31G\*\* basis set carried out by Derrick and co-workers<sup>19</sup> was not compatible with the above experimental result. Through the *ab initio* study at the same level and also at the second-order Møller–Plesset (MP2) perturbation theory level, Øiestad and Uggerud<sup>20</sup> suggested that failure to uniquely identify the critical transition structure is one of the reasons for the above difficulty. Recent *ab initio* study at the MP2 and the quadratic configuration interaction using single and double substitutions (QCISD) levels of theory using the 6-311+G\*\* basis set by Suárez and Sordo<sup>21</sup> displayed single transition states (TS) at each level which are compatible with the above mechanism. Dynamics calculations have been made with a simple analytic theory by Derrick and co-workers<sup>19</sup> and with the direct dynamics method by Øiestad and Uggerud.<sup>20</sup> In the latter, calculation was limited to a single trajectory on the Hartree–Fock (HF) level using the 6-31G\*\* basis set due to the tremendous computational demand and full details of the energy partitioning were not reported.

In the course of our effort to study the product energy partitioning in reaction (1) by classical trajectory calculation on the interpolated PES, we noticed the presence of a bifurcation point (BP)<sup>26–29</sup> on the reaction path. Significance of its position relative to TS, which is level dependent, in dissociation dynamics will be reported in this work. Also reported will be the construction of the interpolated PES incorporating this feature and the classical trajectory study on this surface. Absence of the hydrogen scrambling and the experi-

<sup>a)</sup> Author to whom correspondence should be addressed. Electronic mail: myungsoo@plaza.snu.ac.kr

mental kinetic energy release data will be explained based on the trajectory results.

## II. EXPERIMENT

The laboratory translational kinetic energy profile of the product ion in reaction (1) was measured by the mass-analyzed ion kinetic energy spectrometry (MIKES)<sup>30</sup> using a VG ZAB-E double focusing mass spectrometer with reversed geometry (Micromass Plc, Manchester, UK). Ions were generated by 70 eV electron ionization of methylamine (Aldrich) at the ion source temperature of 180 °C and were accelerated to 8 keV.  $\text{CH}_2\text{NH}_2^+$  from methylamine was selected by the magnetic sector. The kinetic energy spectrum (MIKE spectrum) of the product ion ( $\text{CHNH}^+$ ) generated by the unimolecular dissociation of  $\text{CH}_2\text{NH}_2^+$  inside the dissociation cell located near the intermediate focal point of the instrument was recorded by scanning the electric sector. The cell was floated at a high voltage such that the MIKE peaks due to dissociations occurring inside and outside of the cell could be separated. The time between  $\text{CH}_2\text{NH}_2^+$  formation in the ion source and its dissociation inside the cell was 15.2  $\mu\text{s}$ , which is equivalent to the average rate constant of  $6.6 \times 10^4 \text{ s}^{-1}$ . MIKE profiles from repetitive scans were averaged to obtain data of high quality. Kinetic energy release distributions (KERDs) were obtained by analyzing these profiles using the efficient algorithm developed previously.<sup>31,32</sup> This algorithm corrects all the major discrimination and convolution effects of the instrument and provides an accuracy comparable to the rigorous method based on ion-optical trajectory calculation.<sup>33</sup>

## III. COMPUTATION

Electronic structure calculations were performed for important geometries at the HF, MP2, QCISD, and B3LYP levels with 6-31G\*\* and 6-311+G\*\* basis sets using the GAUSSIAN 98 suite of programs.<sup>34</sup> These include the reactant, structures at the transition states and bifurcation points, intermediates when present, and products. The transition states were identified by the presence of one negative eigenvalue of the Hessian matrix and also by calculating the intrinsic reaction coordinates. Vibrational frequencies were calculated at the optimized geometries also. The global analytic potential for classical trajectory calculations was constructed at the MP2 and HF levels with the 6-31G\*\* and 6-311+G\*\* basis sets, even though most of the results to be presented are those from the MP2/6-311+G\*\* surface. Characteristics along the reaction paths at the MP2, B3LYP, and QCISD levels were qualitatively similar.

Details of the procedure to construct PES for a reaction were reported previously.<sup>14</sup> A brief outline of the procedure is as follows. Using the energy, gradient, and Hessian data obtained by electronic structure calculation at a configuration point, the harmonic approximation of the potential in the vicinity of this point was constructed in the internal coordinate system. Twelve internal coordinates chosen for  $\text{CH}_a\text{H}_b\text{NH}_c\text{H}_d^+$  which loses  $\text{H}_a\text{H}_c$  are as follows, which resulted in fast convergence of dynamics data.<sup>14</sup> Inverses of five interatomic distances,  $r_{\text{H}_a\text{H}_c}^{-1}$ ,  $r_{\text{CH}_a}^{-1}$ ,  $r_{\text{CH}_b}^{-1}$ ,  $r_{\text{NH}_d}^{-1}$ ,  $r_{\text{CN}}^{-1}$ , two

three-atom angles,  $\theta_{\text{CH}_a\text{H}_c}$ ,  $\theta_{\text{NH}_d}$ , and a dihedral angle,  $\phi_{\text{NCH}_a\text{H}_c}$ , were included. In addition, two sets of bending angles,  $(\alpha_1, \beta_1)$  and  $(\alpha_2, \beta_2)$ , were adopted

$$\alpha_1 = \sin^{-1} \left( \frac{\mathbf{r}_{\text{CN}} \times \mathbf{r}_{\text{NH}_a} \cdot \mathbf{r}_{\text{CH}_b}}{r_{\text{CN}} r_{\text{NH}_a} r_{\text{CH}_b}} \right), \quad (2)$$

$$\beta_1 = \cos^{-1} \left( \frac{-\cos(\theta_{\text{NCH}_b})}{\cos \alpha_1} \right), \quad (3)$$

$$\alpha_2 = \sin^{-1} \left( \frac{\mathbf{r}_{\text{CN}} \times \mathbf{r}_{\text{CH}_a} \cdot \mathbf{r}_{\text{NH}_d}}{r_{\text{CN}} r_{\text{CH}_a} r_{\text{NH}_d}} \right), \quad (4)$$

$$\beta_2 = \cos^{-1} \left( \frac{-\cos(\theta_{\text{CNH}_d})}{\cos \alpha_2} \right). \quad (5)$$

$\alpha_1$  and  $\beta_1$  become the out-of-plane and in-plane HCN bending angles of the linear  $\text{CHNH}^+$  product and  $\alpha_2$  and  $\beta_2$  become those for the HNC bendings.  $r_{\text{CH}_b}^{-1}$ ,  $r_{\text{NH}_d}^{-1}$ ,  $r_{\text{CN}}^{-1}$  mentioned above also become internal coordinates of  $\text{CHNH}^+$  in the product region, while  $r_{\text{H}_a\text{H}_c}^{-1}$  is the one for the  $\text{H}_2$  product.

In our original scheme to construct the potential function at  $\mathbf{R}$ ,  $V(\mathbf{R})$ , the configuration points at which the local potentials [ $V^{ij}(\mathbf{R})$ ] had been obtained were classified according to their locations ( $i$ ) with respect to the reaction coordinate. Two types of weighting functions, intraset ( $A_{ij}$ ) and interset ( $B_i$ ), were used to obtain  $V(\mathbf{R})$  as the weighted sum of  $V^{ij}(\mathbf{R})$

$$V(\mathbf{R}) = \sum_i B_i \sum_j A_{ij} V^{ij}(\mathbf{R}). \quad (6)$$

The normalized weight  $A_{ij}$  of the form proposed by Ischtwan and Collins<sup>35</sup> was used

$$A_{ij} = \frac{a_{ij}}{\sum_j a_{ij}}, \quad (7)$$

with

$$a_{ij} = \frac{1}{|\mathbf{R} - \mathbf{R}^{ij}|^{2p}}. \quad (8)$$

Even though the internal coordinates for a many-atom system involved the bond and dihedral angles in addition to the interatomic distances, only the latter were used because the inclusion of angles sometimes produced rather unrealistic results. Recently, it has been found that using only interatomic distances often results in irregular features on the potential energy contour.<sup>36</sup> In this work, we included the angles in the weighting scheme and evaluated  $a_{ij}$  as follows:

$$a_{ij} = \frac{1}{|\mathbf{F}^i \cdot (\mathbf{R} - \mathbf{R}^{ij})|^{2p}}. \quad (9)$$

Here,  $\mathbf{F}^i$  is a vector at the  $i$ th point on the reaction coordinate. Its components are the square roots of the diagonal elements of the Hessian matrix at the point

$$\mathbf{F}^i = (|H_{11}^i|^{1/2}, |H_{22}^i|^{1/2}, \dots, |H_{nn}^i|^{1/2}). \quad (10)$$

Difficulty associated with the difference in units between angles and lengths is eliminated when Eq. (9) is used. Since

$|\mathbf{F}^i \cdot (\mathbf{R} - \mathbf{R}^{ij})|^2$  is proportional to the energy difference between the point of interest and the point where a local potential is known, the energy difference determines the weighting factor in Eq. (9) instead of the geometry difference in Eq. (8). In the case of the interset weight ( $B_i$ ), we retained the original form<sup>14</sup> [similar to Eqs. (7) and (8)] except that the reciprocal distance vector was used instead of  $\mathbf{R}$ . Use of the new weighting scheme substantially improved the energy contour in the case of  $\text{CH}_2\text{OH}^+$  (not shown).

The initial global PES was constructed with local potentials at 40 points on the intrinsic reaction coordinate (IRC) including the reactant, TS, and products. A number of trajectories were run on this PES. One important configuration point was selected from the points sampled on these trajectories. When the quantum-chemically calculated energy at this point differed from the value calculated with the initial PES by more than 0.2 kcal/mol (0.84 kJ/mol), its local potential was added to the initial PES. This process was repeated until a good convergence of dynamics outputs such as the kinetic energy release distribution was achieved, which occurred when 300 off-IRC local potentials were added. As will be shown in the next section,  $\text{H}_d$  and  $\text{H}_c$  become equivalent at the bifurcation point (BP). Namely, there exist two equivalent paths, which are mirror images of each other, connecting BP and reactants,  $\text{CH}_d\text{H}_b\text{NH}_c\text{H}_d^+$  and  $\text{CH}_c\text{H}_b\text{NH}_d\text{H}_d^+$ . To account for the reaction path bifurcation, mirror images of the above 340 local potentials were added, resulting in the interpolated PES consisting of 680 local potentials.

The initial conditions for trajectory runs were selected randomly by orthant-like momentum sampling<sup>8,37</sup> with the molecular geometry fixed at one of the saddle points (TS). Excess energy at the saddle point was taken as the sum of the zero-point energies of vibrations (121.0 kJ/mol at the MP2/6-311+G\*\* level). The orthant-like momentum sampling provides roughly an equal amount of energy for the motion along the reaction path and for each orthogonal vibration. We also attempted normal-mode type samplings. The product mode-specific energies obtained from such trajectories were nearly the same as above, however. The initial rotational angular momentum was selected from the thermal distribution at the ion source temperature (180 °C). The integration of the Hamilton's equations of motion was carried out with Gear's variable order and variable step algorithm<sup>38</sup> until two fragments were 3.3 Å apart. A total of 10 000 trajectories were calculated, about half of which were reactive.

Translational kinetic energy for the relative motion of products, namely KER, was evaluated from atomic positions and momenta at the trajectory end point

$$E_T = \frac{1}{2}\mu |\mathbf{v}_{\text{rel}}|^2. \quad (11)$$

Here,  $\mathbf{v}_{\text{rel}} = \mathbf{v}_{\text{H}_2} - \mathbf{v}_{\text{CHNH}^+}$ .  $\mathbf{v}_{\text{H}_2}$  and  $\mathbf{v}_{\text{CHNH}^+}$  are the center-of-mass velocities of the two products and  $\mu$  is their reduced mass. Calculation of the rotational and vibrational energies of  $\text{H}_2$  is straightforward. The rotational energy of the linear product  $\text{HCNH}^+$  was calculated according to Park *et al.*<sup>39</sup> as

$$E_R = \frac{1}{2}\boldsymbol{\omega}^{2D} \cdot \mathbf{I} \cdot \boldsymbol{\omega}^{2D}. \quad (12)$$

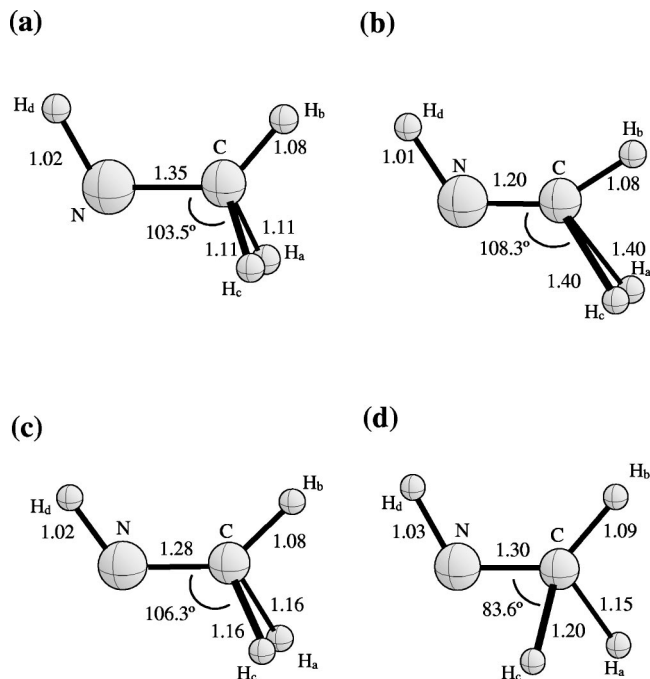


FIG. 1. Structures of saddle points found at the HF/6-31G\*\* [(a)–(c)] and MP2/6-311+G\*\* [(d)] levels. (a) TS1 by Derrick and co-workers (Ref. 19); (b) TS2 by the same investigators which is equivalent to TS2/3+4 by Øiestad and Uggerud (Ref. 20); (c) TS1/2 by Øiestad and Uggerud (Ref. 20); and (d) TS at the MP2/6-311+G\*\* level by Suárez and Sordo (Ref. 21).

Here,  $\boldsymbol{\omega}^{2D}$  is the two-dimensional angular velocity on the plane perpendicular to the principal axis which corresponds to the figure axis at the equilibrium geometry and  $\mathbf{I}$  is the moment of inertia. Mode-specific vibrational energy was calculated in the internal coordinate system using the elimination method<sup>40</sup> for the partial correction of the anharmonicity effect

$$E_{V,l} = \frac{1}{2}\mathbf{v}_l^2 + V(S_0 + \zeta_l \mathbf{G}_0^{1/2} \cdot \boldsymbol{\Lambda}_l) - V(s_0). \quad (13)$$

Here,  $V(\mathbf{s})$  is the potential energy at internal coordinate  $\mathbf{s}$ ,  $s_0$  denotes  $\mathbf{s}$  at the equilibrium geometry,  $\mathbf{v}_l$  is the mass-weighted velocity, and  $\zeta_l \mathbf{G}_0^{1/2} \cdot \boldsymbol{\Lambda}_l$  is the internal displacement vector due to the  $l$ th mode.

## IV. RESULTS AND DISCUSSION

### A. Electronic structure calculations along the reaction path

In the early quantum-chemical study of this reaction at the HF/6-31G\*\* level by Derrick and co-workers,<sup>19</sup> two saddle points were located which were called TS1 and TS2 (Fig. 1). TS1 was reported to be the transition state for the hydrogen exchange between carbon and nitrogen. TS2 was taken as the transition state for 1,1-elimination. Structures at these two transition states were qualitatively similar and could be represented as  $\text{CH}_3\text{NH}^+$ . Derrick and co-workers<sup>19</sup> noted that the transition structures found at this level were not compatible with the synchronous 1,2-elimination established experimentally and suggested that the result was inappropriate due to the neglect of electron correlation effects. Another serious problem in their results was the failure to

find a minimum energy path connecting the reactant and TS2. They suggested that a perambulatory motion near TS1 might push the system over TS2, resulting in dissociation. Quantum-chemical study at the same level, and at the MP2/6-31G\*\* level, was also carried out by Øiestad and Uggerud.<sup>20</sup> They found two transition structures, TS<sup>1</sup>/2 and TS2/3+4 (Fig. 1) in their terminology, which, they claimed, corresponded to TS1 and TS2 in the work of Derrick and co-workers. A stationary point, namely an intermediate, was also found between TS<sup>1</sup>/2 and TS2/3+4. Namely, the critical points on the reaction path were asserted to appear in the order reactant—TS<sup>1</sup>/2—intermediate—TS2/3+4—products. It was also claimed that TS<sup>1</sup>/2 was the critical TS for the reaction in the sense that the system moved irreversibly to the product region once this TS was passed in spite of the presence of the intermediate and the second TS(TS2/3+4). It is confusing to note that the interpretations of the dynamical role of the first TSs differed between the two groups even though Øiestad and Uggerud suggested TS1 and TS<sup>1</sup>/2 are equivalent. Hence, we looked into the detailed structures of these two TSs and found that they were different (Fig. 1). At the same level (HF/6-31G\*\*), we could locate the critical structures reported by Øiestad and Uggerud. A surprising observation was that the structure corresponding to TS1 reported by Derrick and co-workers appeared when IRC was calculated from TS<sup>1</sup>/2 of Øiestad and Uggerud toward the reactant. Along the reaction path from TS1 to the products, the molecule possesses the  $C_s$  symmetry with  $H_a$  and  $H_c$  located at the mirror image positions with respect to the  $CH_bNH_d$  plane. Since the symmetry plane is absent between the reactant and TS1, it is imperative that two reaction paths exist in this region, one leading to the reactant  $CH_aH_bNH_cH_d^+$  and the other to  $CH_cH_bNH_aH_d^+$ . Namely, TS1 is the bifurcation point (BP) of the reaction path. It is also the transition state for the exchange of  $H_a$  and  $H_c$  as reported by Derrick and co-workers,<sup>19</sup> with one negative eigenvalue for the Hessian matrix. A similar bifurcation point was found at the HF/6-311+G\*\* level also. The situation is the same as the appearance of a transition structure/bifurcation point in the isomerization of the methoxy radical.<sup>29</sup> A potential energy contour map calculated at the HF/6-31G\*\* level is drawn in Fig. 2 as a pictorial demonstration of the situation. The potential energy was calculated as a function of distances to  $H_a$  and  $H_c$  from the midpoint of C and N atoms,  $r_{CN-H_a}$  and  $r_{CN-H_c}$ , respectively, with other bond lengths and angles optimized. The fact that the transition structure for hydrogen exchange appears before the reactant arrives at TS<sup>1</sup>/2 at the HF level means that hydrogen scrambling can occur for the reactant before dissociation and is not compatible with the experimental observation of only HD elimination from  $CH_2ND_2^+$ . Then, the suggestion by Øiestad and Uggerud<sup>20</sup> that a specific 1,2-elimination occurred without hydrogen scrambling because TS<sup>1</sup>/2 was the critical TS is not acceptable. The above entrance channel bifurcations do not occur at the MP2, QCISD, and B3LYP levels regardless of the basis set, 6-31G\*\* or 6-311+G\*\*.

Øiestad and Uggerud also observed the second TS, TS2/3+4, and an intermediate located between TS<sup>1</sup>/2 and TS2/3+4 at the HF/6-31G\*\* and MP2/6-31G\*\* levels. We

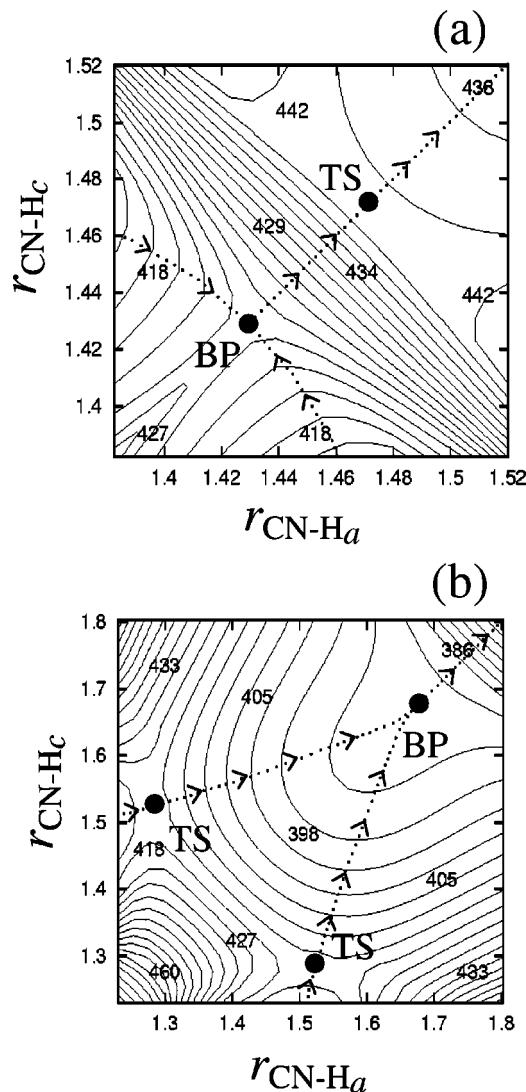


FIG. 2. Potential energy contours on the  $r_{CN-H_a}$ – $r_{CN-H_c}$  plane obtained at the (a) HF/6-31G\*\* and (b) MP2/6-311+G\*\* levels. Positions of the transition states (TS) and bifurcation points (BP) are marked. Broken lines (---) are the minimum energy paths with the arrows indicating the forward direction (from reactant to products) along the reaction path. Numbers denote energy in kJ/mol.

also could find these structures at the same levels and at the QCISD/6-31G\*\* level. However, these were absent at the B3LYP/6-31G\*\* level and at all the levels when the 6-311+G\*\* basis set was used. Namely, only single transition states were found at post-HF levels when the 6-311+G\*\* basis set was used as reported by Suárez and Sordo.<sup>21</sup> The TS structure at the MP2/6-311+G\*\* level is compared with the critical structures obtained at the HF/6-31G\*\* level in Fig. 1. The potential energy diagrams along the reaction path at the HF level with the 6-31G\*\* basis set and MP2, QCISD, and B3LYP levels with the 6-311+G\*\* basis set are drawn in Fig. 3. It is to be noted that the potential energy diagrams at all the levels remain nearly flat after TS and begin to decrease only after the configurations rather similar to TS2 (or TS2/3+4) at the HF level are passed. In each post-HF calculation, a bifurcation point was found at some position on the plateau. Namely, the reflection symmetry appeared at this point and was maintained throughout the exit channel.

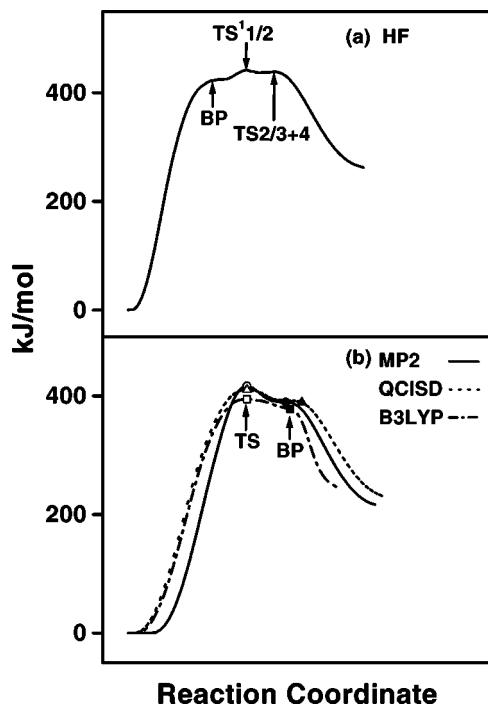


FIG. 3. (a) Potential energy diagram along the reaction path calculated at the HF/6-31G\*\* level. TS<sup>1</sup>/2 and TS<sup>2</sup>/3+4 are the transition states reported by Øiestad and Uggerud (Ref. 20). BP is the bifurcation point which is the same as TS1 reported by Derrick and co-workers (Ref. 19). (b) Corresponding diagrams at the MP2/6-311+G\*\* (—), QCISD/6-311+G\*\* (---), and B3LYP/6-311+G\*\* (---) levels. Transition states at these levels are marked with ○, △, and □, respectively. ●, ▲, and ■ are bifurcation points. Reactant energy minima are taken as the common energy reference. Reaction coordinates (*x* axis) differ for different levels and do not have a quantitative meaning.

These points are marked in Fig. 3. When the BP is located after the TS, another TS which is the mirror image of the one already found must be present, which could be readily confirmed by calculation. The potential energy contour map calculated at the MP2/6-311+G\*\* level is compared with the HF/6-31G\*\* result in Fig. 2. As was reported by Øiestad and Uggerud and also confirmed in our own calculations (*vide*

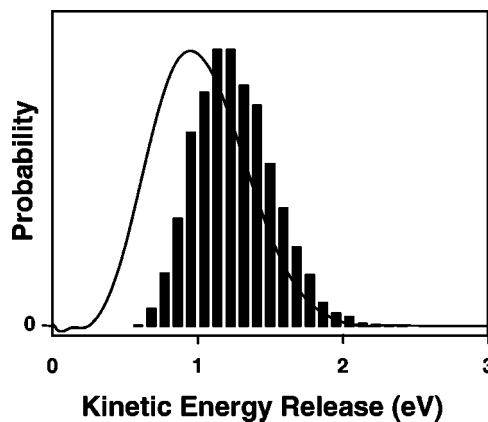


FIG. 4. Experimental (solid curves) and calculated (bar graphs) KERDs for reaction (1).

*infra*), trajectories after passing the TS move almost irreversibly toward the product region. Then, the presence of the bifurcation point after the TS would not result in hydrogen scrambling, in agreement with the results from the deuterium-labeling experiment.<sup>19,23,25</sup> Namely, PESs at the post-HF levels used in this work are qualitatively compatible with the experimental results while the HF surfaces are not.

## B. Experimental KERD and classical trajectory results

The experimental KERD for reaction (1) is shown in Fig. 4. Average KER evaluated from the distribution is 99.1 kJ/mol (1.027 eV). This average is a little larger than the 87.1 kJ/mol (0.903 eV) reported by Derrick and co-workers.<sup>19</sup> Taking  $213 \pm 30$  kJ/mol ( $2.21 \pm 0.31$  eV) reported by Hvistendahl and Uggerud<sup>20</sup> as the experimental reverse barrier, the above average KER is  $46 \pm 6\%$  of the reverse barrier.

The classical reverse barrier ( $E_r^C$ ) obtained by electronic structure calculation at the MP2/6-311+G\*\* level was 203.0 kJ/mol. Adding the zero-point energies at the saddle point to the classical reverse barrier and subtracting the zero-point energies of the products, the quantum-mechanical re-

TABLE I. Reverse barriers and harmonic frequencies of reactant, transition state, and products for reaction (1) calculated at the MP2/6-311+G\*\* level.

Reverse barriers <sup>a</sup>						
$E_r^C$	203.0					
$E_r^Q$	228.2					
Vibrational frequencies <sup>b</sup>						
Reactant	3622	3511	3328	3197	1772	1599
	1475	1356	1162	1096	965	902
TS	3423	3226	2735	2443	1654	1418
	1324	1239	1135	975	657	1079i <sup>c</sup>
CHNH <sup>d</sup>	3655( $\nu_1$ )	3365( $\nu_2$ )	2134( $\nu_3$ )		829( $\nu_4$ )	671( $\nu_5$ )
H <sub>2</sub>			4533			

<sup>a</sup>In kJ/mol.  $E_r^C$  and  $E_r^Q$  are the classical and quantum-mechanical reverse barriers, respectively.

<sup>b</sup>In cm<sup>-1</sup>.

<sup>c</sup>Imaginary frequency along the reaction coordinate.

<sup>d</sup> $\nu_1$ ,  $\nu_2$ , and  $\nu_3$  are NH, CH, and CN stretching vibrations, respectively.  $\nu_4$  and  $\nu_5$  are doubly degenerate HCN and HNC bending vibrations, respectively.

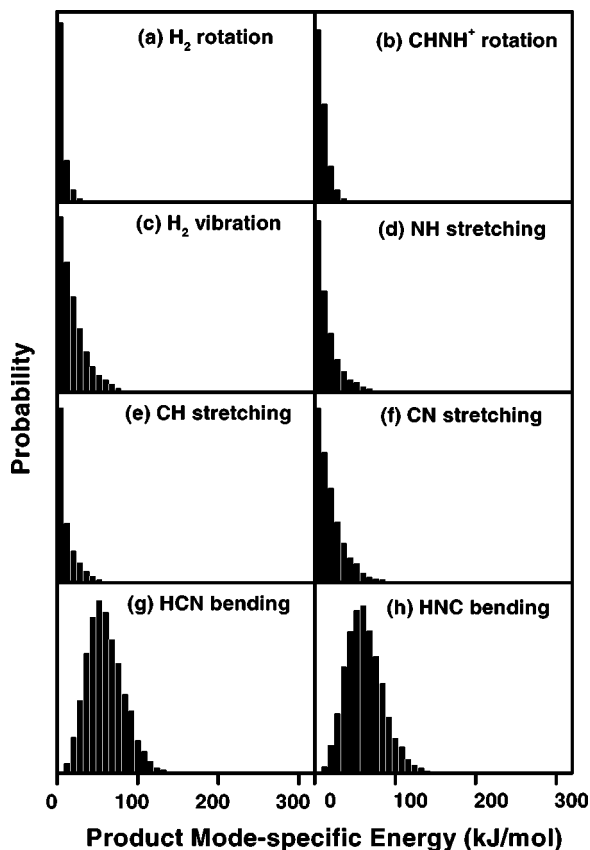


FIG. 5. Distributions of the calculated mode-specific energies for reaction (1). (a) and (b) are for rotations of  $\text{H}_2$  and  $\text{CHNH}^+$ , respectively. (c) is for  $\text{H}_2$  vibration. (d) is for NH stretching ( $\nu_1$ ); (e) CH stretching ( $\nu_2$ ); (f) CN stretching ( $\nu_3$ ); (g) doubly degenerate HCN bending ( $\nu_4$ ); and (h) doubly degenerate HNC bending ( $\nu_5$ ) of  $\text{CHNH}^+$ .

verse barrier ( $E_r^0$ ) was obtained. Vibrational frequencies at the transition state needed for the zero-point energy calculations, and at other geometries also, are listed in Table I. The  $E_r^0$  of 228.2 kJ/mol thus obtained is rather similar to the experimental value of  $213 \pm 30$  kJ/mol.

KERD obtained by trajectory calculation is compared with the experimental data in Fig. 4. The calculated and experimental distributions are similar qualitatively, even though the former shows larger kinetic energy release than the latter. The average kinetic energy release of 123.6 kJ/mol (1.281 eV) evaluated from the calculated distribution is 54% of the available energy ( $E_r^0$ ). This is a little larger than the experimental fraction of  $46 \pm 6\%$ . According to our previous studies<sup>41,42</sup> on the product energy partitioning, such a discrepancy is mainly due to the inaccuracy in the magnitude of the reverse barrier determined by electronic structure calculation. The degree of its inaccuracy is difficult to determine in the present case, however, because the experimental value itself was estimated indirectly and could be erroneous. In addition, one cannot rule out the possibility that the classical nature of the present treatment also contributes to the above discrepancy. Distributions of the mode-specific rotational and vibrational energies for reaction (1) are shown in Fig. 5. Average mode energies evaluated from the distributions are listed in Table II. The product rotational energies of 5.9 and 9.1 kJ/mol ( $493 \text{ cm}^{-1}$  and  $761 \text{ cm}^{-1}$ , respectively) suggest

TABLE II. Experimental kinetic energy release (KER) and calculated product mode-specific energies in kJ/mol. Sum of the calculated mode-specific energies (325.7 kJ/mol) is larger than the available energy ( $E_r^0 = 228.2$  kJ/mol) because the zero-point vibrational energies of the products (95.8 kJ/mol) are included in the former. Minor errors are due to the method used for the mode-specific analysis.

Average KER	Expt. Calc.	99.1 123.6
$\text{CHNH}^+$	Rotation	9.1
	NH stretching ( $\nu_1$ )	15.8
	CH stretching ( $\nu_2$ )	11.0
	CN stretching ( $\nu_3$ )	19.1
	HCN bending ( $\nu_4$ )	59.6
	HNC bending ( $\nu_5$ )	61.8
$\text{H}_2$	Rotation	5.9
	Vibration	19.8

substantial rotational excitation of the products. This occurs because the reaction path does not overlap with the center-of-mass separation vector in the exit channel and fragments spiral for a while during the exit channel motion. Vibrational excitations hardly occurred for the stretching modes of the products, their energies being slightly above or below the zero-point levels. On the other hand, HCN and HNC bending vibrations carried substantial portions of the available energy. Excitation of the bending modes is understandable because vigorous bending motions occur along the exit channel as the system moves from the bent geometry at TS toward the linear geometry in the  $\text{CHNH}^+$  product. Trajectory results on PES constructed at the HF level were qualitatively similar to the MP2/6-311+G\*\* results.

Even though the kinetic energy release of 46% of the available energy in reaction (1) looks substantial, it is smaller than the 75% release in the loss of  $\text{H}_2$  from  $\text{CH}_2\text{OH}^+$ .<sup>8,14</sup> Øiestad and Uggerud<sup>20</sup> suggested that passage over the flat potential energy region between TS<sup>1/2</sup> and TS<sup>2/3+4</sup> in reaction (1) dissipates a significant amount of the available potential energy into internal degrees of freedom other than the translation along the reaction path and results in smaller fraction of KER. To test the validity of such an argument, we also calculated the trajectories initiated at the bifurcation point (Fig. 3) and even further toward the product region using the same total energy as the trajectories initiated at the TS. Energy partitioning data thus obtained were still comparable to those in Table II. Namely, the product kinetic energy originated mostly from the potential energy release in the steep region of the exit channel (see Fig. 3) rather than that in the plateau, in disagreement with the above argument. Inspecting the energy partitioning data in Table II, a simple explanation for the smaller fraction of KER in reaction (1) can be found; the ionic product of reaction (1),  $\text{CHNH}^+$ , has two bending modes to carry away the available energy while only one product bending mode is excited for  $\text{CH}_2\text{OH}^+ \rightarrow \text{CHO}^+ + \text{H}_2$ .<sup>8,14</sup>

We mentioned earlier that even though the reaction path bifurcation occurs at higher levels (MP2/6-311+G\*\*, etc.) also, hydrogen scrambling does not occur in agreement with the experiment because the bifurcation points are located after the TS. If a trajectory which has gone beyond the bifur-

cation point toward the product region comes back to cross the TS toward the reactant, however, the hydrogen scrambling can still occur. In this regard, we counted the number of such trajectories, which was 7 out of 10 000 total trajectories. Namely, hydrogen scrambling hardly occurs as far as BP is located after TS because trajectories seldom reverse their directions during the exit channel motion.

## V. SUMMARY AND CONCLUSION

Recent advances in computational quantum chemistry and reaction dynamics have been useful in elucidating the detailed nature of chemical processes. This has been well demonstrated in the present investigation of the dynamics of H<sub>2</sub> loss from CH<sub>2</sub>NH<sub>2</sub><sup>+</sup>. It has been found that confusion on the critical configurations in the previous reports was caused by the presence of a bifurcation point in the entrance channel at the Hartree–Fock level. Presence of this point, which is also the transition state for hydrogen exchange, before the transition state for dissociation would lead to hydrogen scrambling in complete disagreement with the experimental results. When the electron correlation effect was taken into account at the MP2, QCISD, and B3LYP levels, this bifurcation point moved to the exit channel, namely after the transition state. When the bifurcation point is located after the transition state, hydrogen scrambling may still occur, even though partially, if the trajectory detours at this point and moves back to the reactant region. This was found unlikely through the classical trajectory calculation on a reliable potential energy surface constructed by interpolation of quantum-chemical local potentials.

Classical trajectory calculation was also useful to study the detailed dynamics of this reaction. The experimental kinetic energy release distribution could be adequately reproduced. In addition, the interesting observation that the fraction of the available energy released as the product translational energy is smaller in this reaction than in CH<sub>2</sub>OH<sup>+</sup> → CHO<sup>+</sup> + H<sub>2</sub> could be explained. The classical trajectory result that both of the HCN and HNC bending modes of the ionic product of reaction (1) were highly excited provided the important clue. The capability to calculate product mode-specific energies was especially useful in this regard.

Locating bifurcation points on reaction paths is a subject of great current interest in the field of quantum chemistry. Unlike equilibrium geometries and saddle points, routine computational methods to locate these points are not available in commercial quantum-chemistry software packages. In the present work, we have found bifurcation points based on the symmetry argument (it is well known that bifurcations are often associated with symmetry breaking).<sup>29</sup> Reaction path bifurcations in simple systems like reaction (1) would be useful test cases in the development of systematic algorithms for locating bifurcation points.

## ACKNOWLEDGMENTS

This work was supported financially by CRI, the Ministry of Science and Technology, Republic of Korea. T. H. Choi and S. T. Park thank the Ministry of Education for the Brain Korea 21 fellowship.

- <sup>1</sup>K. Levens, *Fundamental Aspects of Organic Mass Spectrometry* (Verlag Chemie, Weinheim, 1978).
- <sup>2</sup>C. E. Klots, *J. Chem. Phys.* **64**, 4269 (1976).
- <sup>3</sup>W. J. Chesnavich and M. T. Bowers, *J. Chem. Phys.* **66**, 2306 (1977).
- <sup>4</sup>W. J. Chesnavich and M. T. Bowers, *J. Am. Chem. Soc.* **99**, 1705 (1977).
- <sup>5</sup>C. Lifshitz, *Int. J. Mass Spectrom. Ion Processes* **118/119**, 315 (1992).
- <sup>6</sup>I. Powis, *Acc. Chem. Res.* **20**, 179 (1987).
- <sup>7</sup>E. Uggerud and T. Helgaker, *J. Am. Chem. Soc.* **114**, 4265 (1992).
- <sup>8</sup>T. G. Lee, S. C. Park, and M. S. Kim, *J. Chem. Phys.* **104**, 4517 (1996).
- <sup>9</sup>W. Chen, W. L. Hase, and H. B. Schlegel, *Chem. Phys. Lett.* **228**, 436 (1994).
- <sup>10</sup>P. Pechukas and J. C. Light, *J. Chem. Phys.* **42**, 3281 (1965).
- <sup>11</sup>J. C. Light, *Discuss. Faraday Soc.* **44**, 14 (1967).
- <sup>12</sup>L. M. Raff and D. L. Thompson, in *Theory of Chemical Reaction Dynamics*, edited by M. Baer (CRC Press, Boca Raton, 1985), Vol. III.
- <sup>13</sup>G. C. Schatz, M. ter Horst, and T. Takayanagi, in *Modern Methods for Multidimensional Dynamics Computations in Chemistry*, edited by D. L. Thompson (World Scientific, Singapore, 1998).
- <sup>14</sup>Y. M. Rhee, T. G. Lee, S. C. Park, and M. S. Kim, *J. Chem. Phys.* **106**, 1003 (1997).
- <sup>15</sup>S. Y. Lin, S. C. Park, and M. S. Kim, *J. Chem. Phys.* **111**, 3787 (1999).
- <sup>16</sup>T. Taketsugu, N. Watanabe, and K. Hirao, *J. Chem. Phys.* **111**, 3410 (1999).
- <sup>17</sup>M. A. Collins and D. H. Zhang, *J. Chem. Phys.* **111**, 9924 (1999).
- <sup>18</sup>Y. M. Rhee and M. S. Kim, *J. Chem. Phys.* **109**, 5363 (1998).
- <sup>19</sup>K. F. Donchi, B. A. Rumpf, G. D. Willett, J. R. Christie, and P. J. Derrick, *J. Am. Chem. Soc.* **110**, 347 (1988).
- <sup>20</sup>Å. M. L. Øiestad and E. Uggerud, *Int. J. Mass Spectrom. Ion Processes* **167/168**, 117 (1997).
- <sup>21</sup>D. Suárez and T. L. Sordo, *J. Phys. Chem. A* **101**, 1561 (1997).
- <sup>22</sup>S. Sæbø, *Chem. Phys. Lett.* **47**, 564 (1997).
- <sup>23</sup>D. H. Williams and G. Hvistendahl, *J. Am. Chem. Soc.* **96**, 6753 (1974).
- <sup>24</sup>E. Uggerud, *Mass Spectrom. Rev.* **18**, 285 (1999).
- <sup>25</sup>G. Hvistendahl and E. Uggerud, *Org. Mass Spectrom.* **20**, 541 (1985).
- <sup>26</sup>W. Quapp, M. Hirsch, and D. Heidrich, *Theor. Chem. Acc.* **100**, 285 (1998).
- <sup>27</sup>P. Valtazanos and K. Ruedenberg, *Theor. Chim. Acta* **69**, 281 (1986).
- <sup>28</sup>H. B. Schlegel, *J. Chem. Soc., Faraday Trans.* **90**, 1569 (1994).
- <sup>29</sup>M. Ramquet, G. Dive, and D. Dehareng, *J. Chem. Phys.* **112**, 4923 (2000).
- <sup>30</sup>R. G. Cooks, J. H. Beynon, R. M. Caprioli, and G. R. Lester, *Metastable Ions* (Elsevier, Amsterdam, 1973).
- <sup>31</sup>I. C. Yeh and M. S. Kim, *Rapid Commun. Mass Spectrom.* **6**, 115 (1992).
- <sup>32</sup>I. C. Yeh and M. S. Kim, *Rapid Commun. Mass Spectrom.* **6**, 293 (1992).
- <sup>33</sup>T. Matsuo, H. Matsuda, Y. Fujita, and H. Wollnik, *Mass Spectrosc. (Tokyo)* **24**, 19 (1976).
- <sup>34</sup>M. J. Frisch, G. W. Trucks, H. B. Schlegel *et al.*, GAUSSIAN 98, Revision A.6, Gaussian, Inc., Pittsburgh, PA, 1998.
- <sup>35</sup>J. Ischtwan and M. A. Collins, *J. Chem. Phys.* **100**, 8080 (1994).
- <sup>36</sup>Y. M. Rhee, *J. Chem. Phys.* **113**, 6021 (2000).
- <sup>37</sup>D. L. Bunker and W. L. Hase, *J. Chem. Phys.* **59**, 4621 (1973).
- <sup>38</sup>G. Hall and J. M. Watt, *Modern Numerical Methods for Ordinary Differential Equations* (Clarendon, Oxford, 1976).
- <sup>39</sup>S. T. Park, J. H. Moon, and M. S. Kim, *J. Chem. Phys.* **107**, 9899 (1997).
- <sup>40</sup>Y. M. Rhee and M. S. Kim, *J. Chem. Phys.* **107**, 1394 (1997).
- <sup>41</sup>J. H. Moon, S. T. Park, and M. S. Kim, *J. Chem. Phys.* **110**, 972 (1999).
- <sup>42</sup>B. J. Sung and M. S. Kim, *J. Chem. Phys.* **113**, 3098 (2000).